Japanese Journal of Applied Physics

REGULAR PAPER

Composition dependence of structural and piezoelectric properties in $Bi(Mg_{0.5}Ti_{0.5})O_3$-modified $BaTiO_3$-$BiFeO_3$ ceramics

To cite this article: Hyunwook Nam *et al* 2022 *Jpn. J. Appl. Phys.* **61** SN1033

Japanese Journal of Applied Physics **61**, SN1033 (2022) **REGULAR PAPER**
https://doi.org/**10.35848/1347-4065/ac85c7**

Composition dependence of structural and piezoelectric properties in Bi$(Mg_{0.5}Ti_{0.5})O_3$-modified $BaTiO_3$-$BiFeO_3$ ceramics

Hyunwook Nam[1], Ichiro Fujii[1], Sangwook Kim[2], Takaaki Ishii[1], Shintaro Ueno[1], Gopal Prasad Khanal[1], Yoshihiro Kuroiwa[2], and Satoshi Wada[1*]

[1]*Graduate Faculty of Interdisciplinary Research, University of Yamanashi, Kofu, Yamanashi 400-8510, Japan*
[2]*Graduate School of Advanced Science and Engineering, Hiroshima University, Higashihiroshima, Hiroshima 739-8526, Japan*

[*]E-mail: swada@yamanashi.ac.jp

Received June 12, 2022; revised July 23, 2022; accepted August 1, 2022; published online August 25, 2022

The chemical composition dependence of the Bi$(Mg_{0.5}Ti_{0.5})O_3$ (BMT)-modified $BaTiO_3$ (BT)-$BiFeO_3$ (BF) ceramics fabricated by a solid-state synthesis was studied. The effects of BT/BF ratios and BMT concentration on the crystal structure, piezoelectric, and ferroelectric properties were investigated. The crystal structure study carried out under the synchrotron radiation X-ray diffraction revealed a change from rhombohedral structure to the pseudo-cubic structure when the BT contents were increased. A significant change in crystal structure and piezoelectric characteristics was confirmed by varying the BT/BF ratios. In contrast, the crystal symmetry remained unaffected by varying the BMT concentration, while tailoring of the piezoelectric and ferroelectric properties was revealed. Based on the analysis of the structural characteristics and overall electrical properties, the ceramics with modification of the BMT content along with BT/BF ratios could be applied as candidate materials for various practical applications. © 2022 The Japan Society of Applied Physics

1. Introduction

Lead zirconate titanate (PZT) solid solution has been widely used owing to its outstanding dielectric and piezoelectric properties, especially with composition in the vicinity of a morphotropic phase boundary (MPB).[1–3] Regarding the origin of the excellent piezoelectric response in PZT, it is reported that the domain structure near the MPB region is composed of nanometer domains, and those nano-sized domains are the key point for high piezoelectric performance.[4,5] Similarly, a significantly increased piezoelectric response has also been reported in other lead-based systems with decreasing domain size.[6,7] Thus, the fabrication of a piezoelectric ceramics system consisting of nano-sized domains with static polar vectors is necessary for achieving high performance. Recently, lead-free piezoelectric ceramics have been extensively investigated to reduce hazardous waste and harmful materials for a future eco-friendly environment. Thus, lead-free piezoelectric ceramics containing the desired nano-sized domain structure are a noticeable issue.

$BiFeO_3$ (BF)-based lead-free piezoelectric ceramics are gaining interest owing to their high Curie temperature (T_c). When the typical ferroelectric BF is introduced to the relaxor-like materials, nano-sized domains with static polar vectors are expected to be achieved similar to that in relaxor ferroelectrics. Relaxor-like $BaTiO_3$-Bi$(Mg_{0.5}Ti_{0.5})O_3$ (BT-BMT) materials were reported to be suitable starting candidates due to their polar nano regions with flipping polar vectors.[8,9] It was found that the nano-sized domain structure and ferroelectric-like domain structure can be tuned by chemical composition in the BT-BMT-BF system.[10–14] For instance, a relatively BT- and BMT-rich composition exhibited a nano-sized domain with relaxor-like behavior, while a BF-rich composition consisted of a macro-sized domain with ferroelectric nature.[11,12] However, the detailed study of chemical composition dependence over a wide range of structural, piezoelectric, and ferroelectric properties in the BT-BMT-BF system has not been reported yet. In addition, the phase transition temperature in the BF-rich composition is also unclear to date. In this work, the effect of various chemical compositions on structural and various electrical properties was systematically studied with varying BT/BF ratios and BMT concentrations. The piezoelectric and ferroelectric properties, and the phase transition temperature were confirmed by various electrical properties and high-energy synchrotron radiation X-ray diffraction (SR-XRD). For this purpose, the material system with composition of $1\text{-}y\{(1\text{-}x)BF\text{-}xBT\}$ yBMT, where $0.25 \leqslant x \leqslant 0.40$ and $0.01 \leqslant y \leqslant 0.10$, were selected for which the compositional map is shown in Fig. 1.

2. Experimental methods

The chemical compositions, $1\text{-}y\{(1\text{-}x)BiFeO_3\text{-}xBaTiO_3\}y$ Bi$(Mg_{0.5}Ti_{0.5})O_3$ with $x = 0.25$, 0.30, 0.33, 0.40 (referred to as 25BTBF, 30BTBF, 33BTBF, and 40BTBF) and $y = 0.01$, 0.03, 0.05, 0.10 (referred to as 1BMT, 3BMT, 5BMT, and 10BMT), were prepared using $BaTiO_3$ (BT, Sakai Chemical Industry Co., LTD), $BiFeO_3$ (BF, Nippon Chemical Industrial Co., LTD), Bi_2O_3 (99.999%, Rare Metallic Co., LTD), MgO (99.9%, Rare Metallic Co., LTD), and TiO_2 (99.98%, Ishihara Sangyo Kaisha, LTD) powders. The starting powders were mixed through ball milling for 24 h, and calcined at 800 °C for 6 h. Then, second ball milling was performed and dried at 80 °C. A polyvinyl butyral (PVB) binder was added to the dried powders, and green disk pellets were formed by uniaxial pressing at 250 MPa. After performing the binder burnout at 700 °C for 10 h, the pellets were sintered at 990 °C– 1010 °C for 4 h in the air (990 °C for 25BTBF-BMT series, 1000 °C for 30BTBF-BMT and 33BTBF-BMT series, and 1010 °C for 40BTBF-BMT series). The crystal structure was investigated by an X-ray diffractometer (XRD, Ultima IV, Rigaku) with Cu Kα radiation and SR-XRD in the SPring-8. A temperature-dependent SR-XRD measurement was carried out only for the 25BTBF-BMT series. For microstructure observation by scanning electron microscopy (SEM, JSM-6510, JEOL), the ceramics were mirror-polished and chemically etched using 1 N HCl solution for 20 min. The sintered pellets were polished and were cut to a size of 4 mm (length) ∗ 1.5 mm (width) ∗ 0.4 mm^3 (thickness) for electrical properties measurement. The prepared samples were annealed at 800 °C for 20 h and were subsequently quenched in water. The quenching process was carried out to enhance the domain wall motion by the effects of domain wall de-pinning.[10,15–17] Gold electrodes

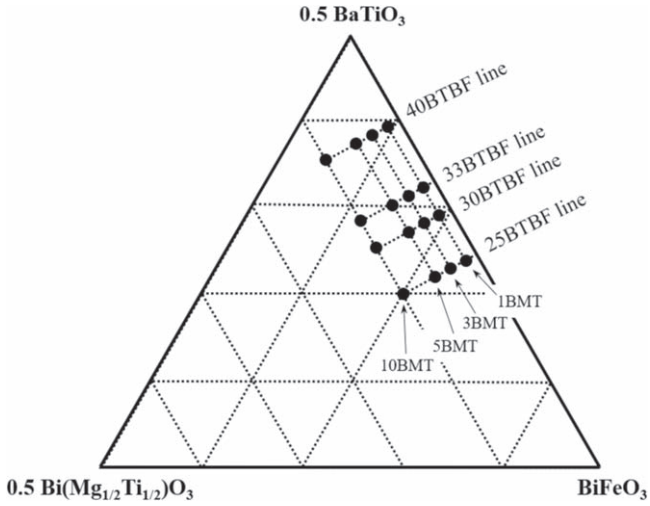

Fig. 1. The schematic composition map of 1-y\{(1-x)$BiFeO_3$$xBaTiO_3$\} $yBi(Mg_{0.5}Ti_{0.5})O_3$ solid solution, with $x = 0.25$, 0.30, 0.33, 0.40 (referred to as 25BTBF, 30BTBF, 33BTBF, and 40BTBF) and $y = 0.01$, 0.03, 0.05, 0.10 (referred to as 1BMT, 3BMT, 5BMT, and 10BMT).

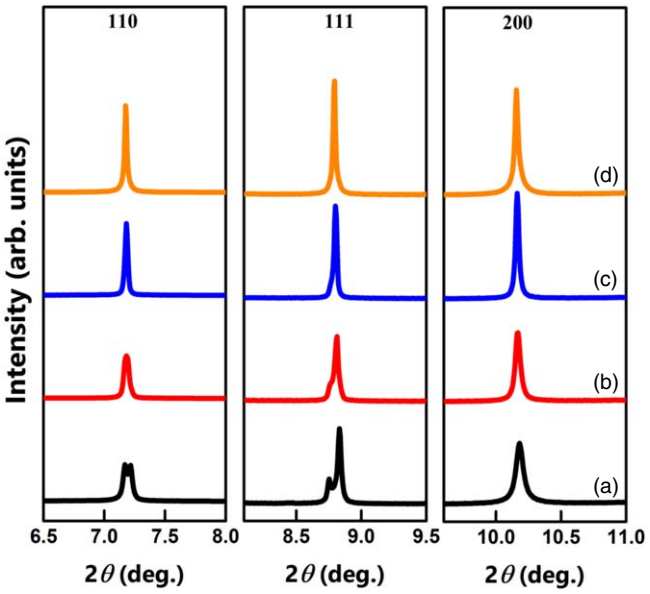

Fig. 2. (Color online) The SR-XRD patterns showing 110, 111, and 200 peaks for 10BMT-modified BTBF series: (a) 25BTBF-10BMT, (b) 30BTBF-10BMT, (c) 33BTBF-10BMT, and (d) 40BTBF-10BMT.

were coated on the surfaces of the samples and heated at 300 °C for 10 min. The temperature dependence of the dielectric constant and loss was measured by an LCR analyser (6440B, Wayne Kerr Electronics) in the range of 20 °C–500 °C. Polarization–electric field (P–E) loops and strain–electric field (s–E) curves were determined using a ferroelectric and strain measuring system (JP005-SE, Kitamoto Denshi) with a displacement meter (Millitron 1202IC, Mahr), which was measured at 0.1 Hz at room temperature. The quenched 0.5 mm (length) ∗ 0.5 mm (width) ∗ 1.5 mm^3 (thickness) samples were poled under the DC electric field of 45 kV cm^{-1} at room temperature for 5 min, and were measured using an impedance analyzer (4192 A, YHP). The small-signal piezoelectric constant (d_{33}) was measured by a d_{33} meter (PiezoMeter PM300, Piezotest), and it was also calculated by the resonance-antiresonance method.

3. Results and discussion

The crystal structures of samples with 10BMT and various BT/BF ratios were measured by SR-XRD. Typical perovskite structure without the secondary phase was observed for all compositions as shown in Fig. 2 and Appendix A. It has been reported that the crystal structure of (1-x)BF-xBT system is the rhombohedral structure for BF-rich composition ($x \leqslant 0.25$), and for the composition with $x \geqslant 0.30$, it changes to the pseudo-cubic structure.[18] Variation of crystal structures by changing BT/BF ratios was also reported for various BF-based piezoelectric ceramics.[18,19] Moreover, crystal structure in BF-based solid solution ceramics is also dependent on the synthesis process and other various reasons.[20,21] Thus, investigation of crystal structure with varying concentrations of BT contents is crucial in BF-based solid solution ceramics. A distinctly separated peak was observed in 111 peak of the 25BTBF-10BMT system which corresponds to a rhombohedral structure. Similarly, a shoulder-like peak was also seen in 111 peak for 30BTBF-10BMT composition, while the 200 peaks revealed single peak in both 25BTBF-10BMT and 30BTBF-10BMT compositions. Here, it should be mentioned that the crystal structure of 30BTBF-10BMT is difficult to clearly define its crystal symmetry as rhombohedral because of its broad 111 peak. Previous literature has assigned the crystal structure of the material system with similar XRD patterns by the investigation of temperature-dependent SR-XRD measurement as the rhombohedral structure.[18] On the other hand, the 33BTBF-10BMT and 40BTBF-10BMT series showed no peak splitting for all the 110, 111, and 200 peaks, thereby suggesting its crystal structure to be cubic. However, typical piezoelectric properties were observed in this symmetry, hence it is not an ideal cubic symmetry, instead, it is generally referred to as a pseudo-cubic structure. In addition, the crystal structure for the 33BTBF-10BMT composition was clearly confirmed as the pseudo-cubic structure in our previous report.[22,23] Thus, the crystal structure is changed from rhombohedral to pseudo-cubic structure with increasing the BT contents as shown in Fig. 2 and Appendix A.

The ferroelectric and piezoelectric properties were investigated from P–E hysteresis loops, and bipolar and unipolar s–E curves, which were measured at 0.1 Hz at room temperature as shown in Figs. 3–5. In addition, various property parameters of the BMT-modified BTBF systems studied in this paper has been summarized in Table I. Based on the P–eE hysteresis loops, a large remanent polarization (P_r) and coercive field (E_c) were observed in BF-rich compositions such as for the 25BTBF-BMT lines as shown in Fig. 3. With increasing the BT contents, P_r was decreased from 38 μCcm^{-2} for 25BTBF-10BMT to 15 μCcm^{-2} for 40BTBF-10BMT, furthermore the E_c value was also decreased by approximately two folds from 38 kV cm^{-1} to 18 kV cm^{-1}, as shown in Table I, respectively. The 25BTBF-BMT series exhibited high E_c that are typical hard-type piezoelectric material. In contrast, the 40BTBF-BMT series showed significantly low E_c. It is well reported that typical hard piezoelectric ceramics show pinched P–E hysteresis loops due to the domain wall pinning, which could be changed to typical open P–E hysteresis loops after electric field cycling.[24] However, a well-saturated square-shaped P–E hysteresis loop obtained for the 25BTBF-BMT series is attributed to the domain wall de-pinning effect that was

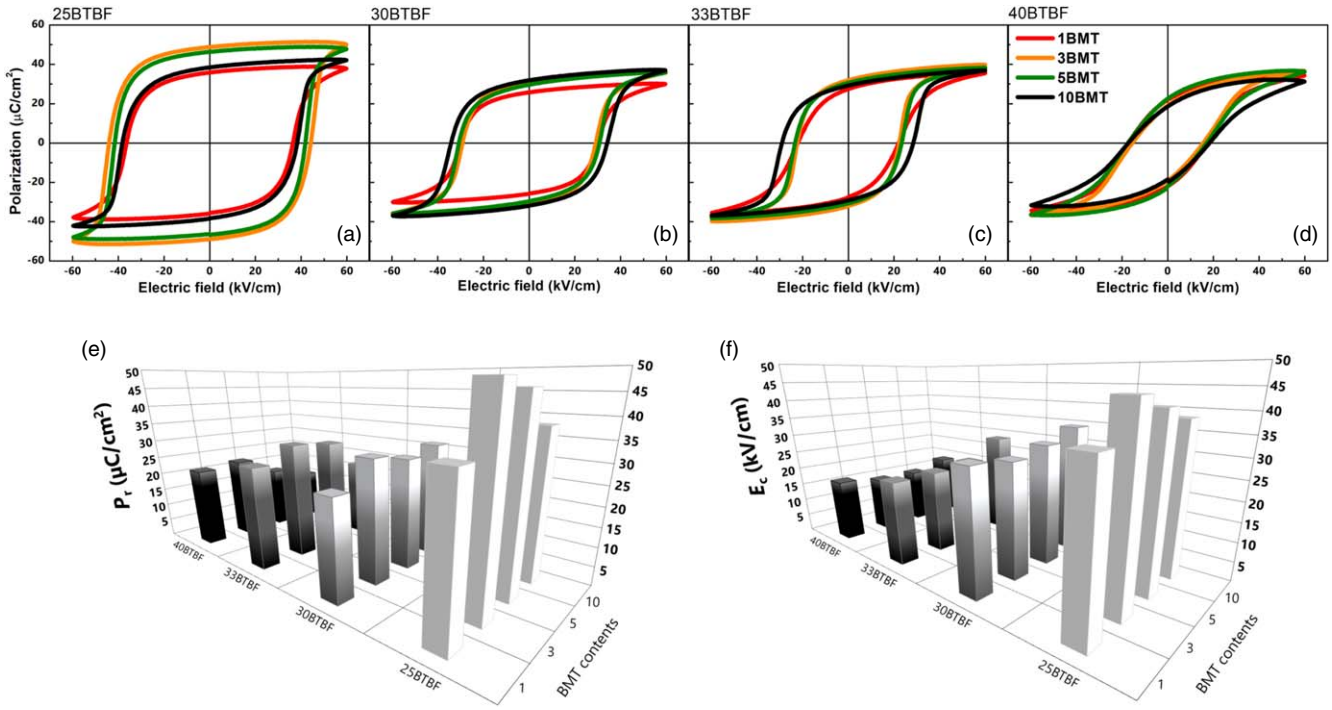

Fig. 3. (Color online) The polarization–electric field (P–E) hysteresis loops for BMT-modified BTBF solid solution: (a) 25BTBF-BMT series, (b) 30BTBF-BMT series, (c) 33BTBF-BMT series, and (d) 40BTBF-BMT series. (e) Remanent polarization, P_r, and (f) coercive field, E_c of each composition.

Table I. The summary of various property parameters of the BMT-modified BTBF systems.

Composition	Grain size (μm)	P_r(μCcm^{-2})	E_c(kV/cm)	ε_r(1 kHz)	tan δ(1 kHz)	T_{max} (°C)	Bipolar S_{max} (%)
25BTBF-1BMT	2.1 ± 0.9	35	36	466	0.028	625	0.07
25BTBF-3BMT	1.8 ± 0.3	48	44	453	0.035	630	0.09
25BTBF-5BMT	1.9 ± 0.3	46	41	456	0.037	677	0.08
25BTBF-10BMT	2.1 ± 0.3	38	38	445	0.033	682	0.10
30BTBF-1BMT	2.6 ± 1.0	25	30	684	0.066	471	0.12
30BTBF-3BMT	2.7 ± 0.9	31	29	581	0.066	498	0.14
30BTBF-5BMT	2.6 ± 1.1	29	31	741	0.065	483	0.10
30BTBF-10BMT	2.5 ± 0.4	31	34	636	0.070	499	0.14
33BTBF-1BMT	2.5 ± 0.7	27	22	853	0.079	429	0.17
33BTBF-3BMT	3.0 ± 0.8	31	22	946	0.084	450	0.17
33BTBF-5BMT	2.4 ± 0.6	30	23	794	0.082	453	0.18
33BTBF-10BMT	3.1 ± 0.7	32	28	704	0.084	465	0.17
40BTBF-1BMT	2.9 ± 0.3	22	17	729	0.090	378	0.22
40BTBF-3BMT	2.5 ± 0.6	23	16	918	0.101	331	0.22
40BTBF-5BMT	2.5 ± 0.5	18	16	849	0.097	363	0.19
40BTBF-10BMT	2.1 ± 0.3	15	18	813	0.093	381	0.18

	γ	Unipolar S_{max} (%)	d_{33}* (pm/V)	Strain hysteresis (%)	d_{33}-meter (pC/N)	d_{33}-resonance (pC/N)	θ_{max} (°)
25BTBF-1BMT	—	0.11	184	29	53	—	—
25BTBF-3BMT	—	0.11	180	27	123	—	—
25BTBF-5BMT	—	0.10	173	26	105	—	—
25BTBF-10BMT	—	0.11	178	28	84	—	—
30BTBF-1BMT	1.61	0.17	283	20	127	86	32
30BTBF-3BMT	—	0.15	249	16	130	—	—
30BTBF-5BMT	1.66	0.16	261	19	134	96	42
30BTBF-10BMT	—	0.17	287	22	119	98	7
33BTBF-1BMT	1.75	0.19	290	16	—	—	—
33BTBF-3BMT	1.87	0.18	302	11	128	105	33
33BTBF-5BMT	1.74	0.19	310	12	142	90	39
33BTBF-10BMT	1.77	0.17	286	13	120	120	23
40BTBF-1BMT	1.97	0.23	384	18	40	—	—
40BTBF-3BMT	1.97	0.22	370	22	40	—	—
40BTBF-5BMT	1.99	0.19	318	17	30	—	—
40BTBF-10BMT	1.98	0.20	341	18	35	—	—

achieved by tailoring point-defect distribution through the quenching treatment.[10,15–17,25,26] The $(Bi_{0.5}Na_{0.5})TiO_3$ (BNT)-based piezoelectric ceramics are a potential candidate for high-power applications owing to their high E_c, which possibly maintains high mechanical reliability.[27,28] Similarly, BF-rich systems such as the 25BTBF-BMT series showed high E_c. Thus, it could be taken as a candidate system for the high-power application, if the mechanical quality factor is reliable in this system. Therefore, investigation of mechanical quality factors and other mechanical characterization for high-power application in this material system would be noteworthy.[27–29]

The maximum strain (S_{max}) and negative strain (S_{neg}) values are plotted for bipolar *s–E* curves of BMT-modified BTBF systems with various compositions as shown in Fig. 4. S_{max} was gradually increased when increasing the BT contents, while S_{neg} was dramatically decreased. It can be noted that for the 25BTBF-BMT line, S_{neg} varied in the range of 0.209%–0.295%, whereas it ranged from 0.025 to 0.065% for the 40BTBF-BMT line. Such a large negative strain of the 25BTBF-BMT composition series diminished the capability of showing large strains upon unipolar loading, and the resultant trade-off behavior can be seen in Figs. 4 and 5. It is well known that the large-signal piezoelectric constant (d_{33}*, calculated by S_{max}/E_{max} from unipolar *s–E* curves) is one of the key parameters for the piezoelectric actuator. Figure 5 shows the unipolar *s–E* curves of various compositions measured at an electric field of 60 kVcm^{-1}. The d_{33}* varied in the range of 173–184 pm V^{-1} for 25BTBF-BMT series, 249–287 pm V^{-1} for 30BTBF-BMT series, 286–310 pm V^{-1} for 33BTBF-BMT series, and 318–384 pm V^{-1} for 40BTBF-BMT series as shown in Table I. A relatively large strain and d_{33}* over 300 pm V^{-1} were obtained in the 33BTBF-BMT and 40BTBF-BMT lines. The BNT-based lead-free piezoelectric ceramics are one of the potential candidates for actuator devices owing to their giant strain, but their practical applications might be difficult because of large strain hysteresis which is approximately over 50%.[30,31] Based on unipolar *s–E* curve results, comparably low strain hysteresis was observed in all the 30BTBF-BMT, 33BTBF-BMT, and 40BTBF-BMT series. It is relatively a low strain hysteresis value compared to other lead-free piezoelectric ceramics. As mentioned earlier, large S_{neg} removes the capability of large strain upon unipolar loading. In general, the magnitude of S_{neg} is interrelated with the domain switching process. In a BF-based solid solution system, easier domain back-switching is exhibited when the BT content was increased, and it might be related to the predominant relaxor characteristics with nano-sized domain structure.[32]

Strong frequency dispersion in the temperature dependence of dielectric constant measurement is well reported for the relaxor-like material system. Thus, the understanding of dielectric relaxation by the temperature dependence of the dielectric constant is required. In addition, the information on the phase transition temperature on BMT-modified BTBF ceramics over a wide range of chemical composition dependence can be observed simultaneously. The tendency of dielectric relaxation and temperature of maximum dielectric constant (T_{max}) are plotted by the temperature dependence of the dielectric constants and losses as shown in Fig. 6, Table I, and Appendix B. Only, the 25BTBF-BMT series did not reveal T_{max} up to 500 °C, which was confirmed by temperature-dependent SR-XRD as shown in Appendix C and Table I. The highest T_{max}, with the range of 620 °C–682 °C, was seen for the 25BTBF-BMT series. The T_{max} gradually decreased with increasing the BT contents, and the lowest T_{max} was shown by the 40BTBF-BMT series, which varied in the range of 330 °C–381 °C. This is simply because of the nature of the low Curie temperature of BT ($T_c \approx 130$ °C). However, although the 40BTBF-BMT series shows the lowest T_{max} among all of the studied compositions,

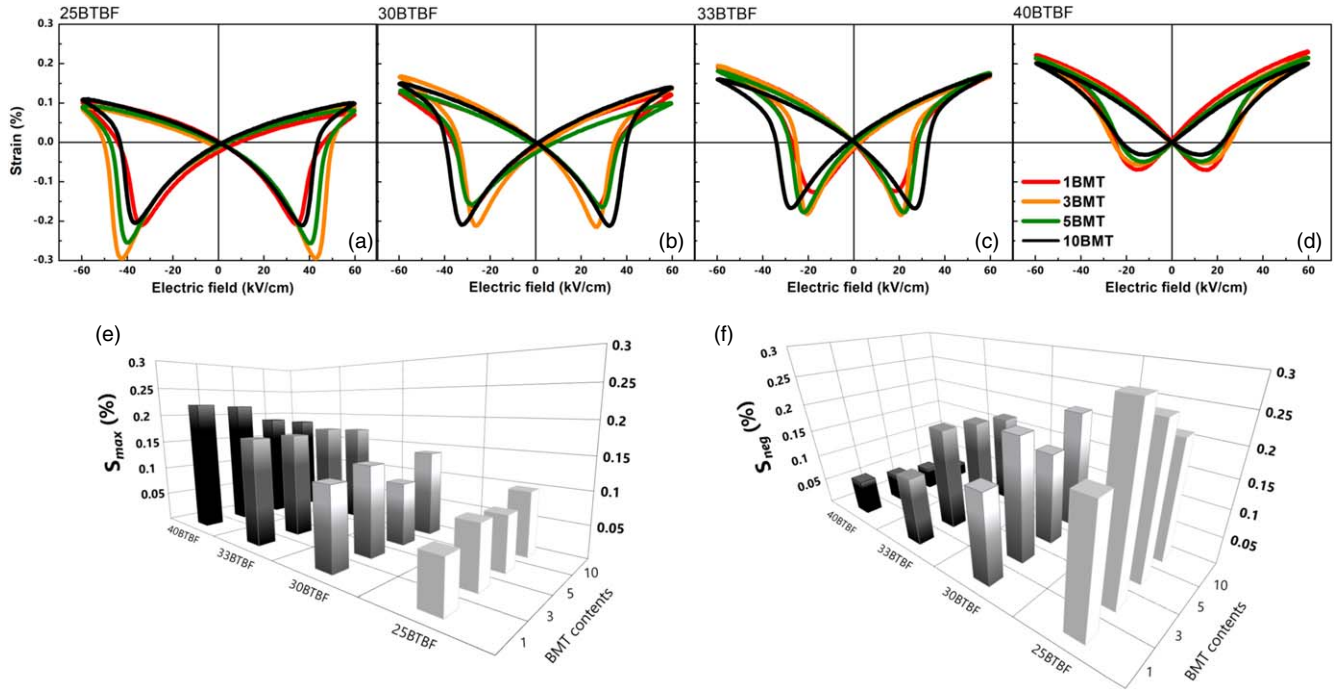

Fig. 4. (Color online) The bipolar strain–electric field (*s–E*) curves for BMT-modified BTBF solid solution: (a) 25BTBF-BMT series, (b) 30BTBF-BMT series, (c) 33BTBF-BMT series, and (d) 40BTBF-BMT series. (e) Maximum strain, S_{max}, and (f) negative strain, S_{neg} of each composition.

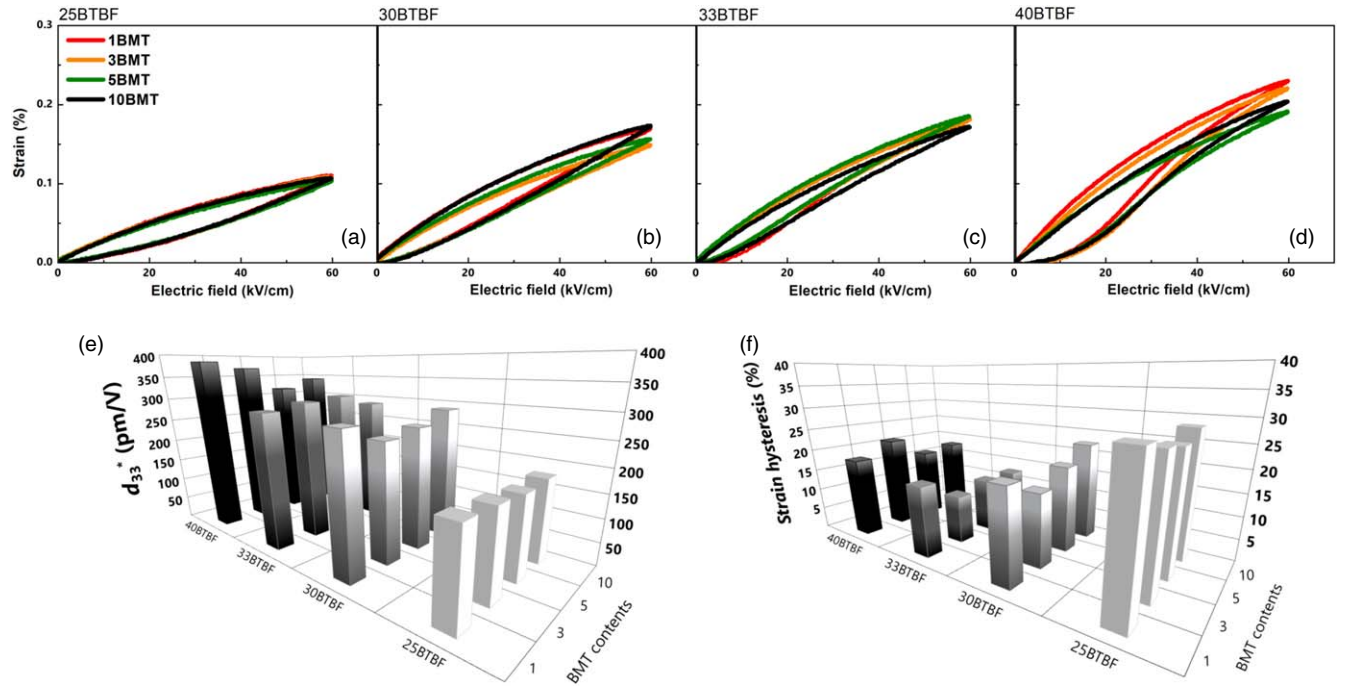

Fig. 5. (Color online) The unipolar strain–electric field (*s*–*E*) curves for BMT-modified BTBF solid solution: (a) 25BTBF-BMT series, (b) 30BTBF-BMT series, (c) 33BTBF-BMT series, and (d) 40BTBF-BMT series. (e) d_{33}* and (f) strain hysteresis of each composition.

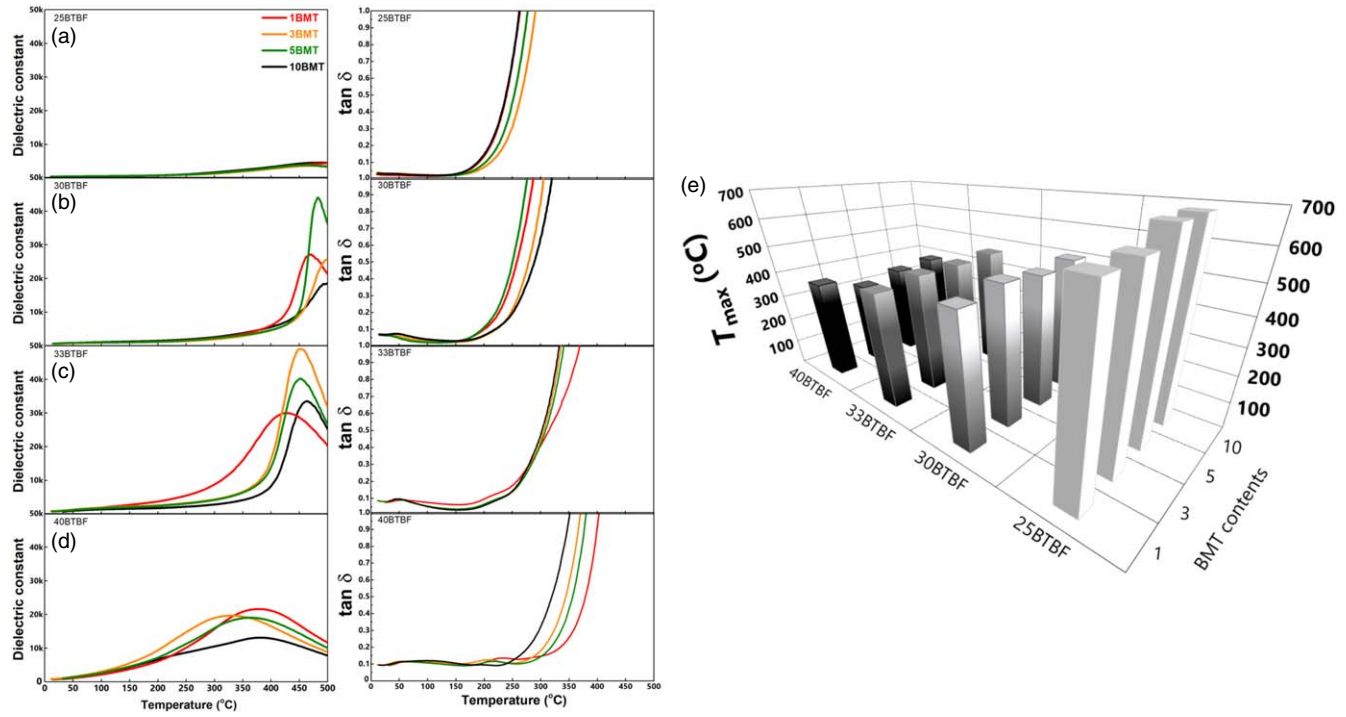

Fig. 6. (Color online) Temperature dependence of dielectric constants and losses for BMT-modified BTBF solid solution: (a) 25BTBF-BMT series, (b) 30BTBF-BMT series, (c) 33BTBF-BMT series, and (d) 40BTBF-BMT series at 1 kHz. (e) Temperature of maximum dielectric constant, T_{max} of each composition.

it is relatively higher than that of the commonly used soft and hard PZT ceramics.[33,34] Dielectric losses for all the compositions do not increase dramatically until 150 °C. However, a dramatic increase in dielectric loss was observed for each composition above a certain temperature. The temperature for the dramatic increase in the dielectric loss is higher for samples with higher BT contents, which is considered to be related to the suppression of oxygen vacancies due to the lower BF contents. The dramatic increase in the dielectric loss at high temperatures due to high electrical conductivity originated from higher concentration of oxygen vacancies in BF based systems has been reported in several BTBF systems in general.[10,19,35,36] Dielectric relaxation is one of the key characteristics of relaxor-like ceramics. To further understand this characteristic, a modified Curie–Weiss law was applied and it can be expressed as the following equation:

$$\frac{1}{\varepsilon} - \frac{1}{\varepsilon_m} = \frac{(T - T_{max})^{\gamma}}{C}$$

where ε_m is the maximum dielectric constant at T_{max}, C is a constant, and γ is the degree of diffuseness.[37] Here, the γ value is in the range of 1 to 2 ($\gamma = 1$ corresponds to typical ferroelectrics and $\gamma = 2$ corresponds to relaxors). The fitted γ values are in the range of 1.61–1.66 for the 30BTBF-BMT series, 1.74–1.86 for the 33BTBF-BMT series, and 1.92–1.99 for the 40BTBF-BMT series, as shown in Table I. The gradual increment of the γ value indicated that the relaxor characteristic is getting dominant with increasing the BT content. Hence, the effect of the BT/BF ratio is strongly related to the dominant relaxor order. The BF-rich composition such as the 25BTBF-BMT series show rhombohedral symmetry and strong ferroelectric order, however, the addition of a higher concentration of BT appears to disrupt the dominant ferroelectric order. This tendency becomes dominant in BT-rich compositions such as the 40BTBF-BMT series, leading to the pseudo-cubic symmetry, low P_r, E_c, and S_{neg}, but large d_{33}*. Hence, the BF-rich and BT-rich series with varying characteristics depending on composition dependence might be considered for various practical applications. Dielectric relaxation as a function of the frequency on the temperature-dependent dielectric constant seen in the relaxor ferroelectrics is also reported in other BTBF-based systems.[10,18,19,25,36] Furthermore, the combination of relaxor-like BT-BMT with nano-sized domains and ferroelectric BF with macro-sized domains is similar to the complex domain structure exhibited by several BTBF-based relaxor ferroelectrics.[11,12,14,32,38] Based on the analysis of the structural characteristics and overall electrical properties, the 33BTBF-BMT series was found to be a relaxor ferroelectric characteristics with pseudo-cubic crystal symmetry. Here, a relatively high small-signal d_{33} was achieved at 33BTBF-BMT series among all of the studied compositions. Although still low small-signal d_{33} and difficulty of poling (simply estimated by phase angle) are the current limitations for this system as shown in Table I, the alternating current poling (ACP) rather than the DCP process could be one of the strategies to overcome the current limitation. Recently, it was suggested that ultrahigh piezoelectric properties have been reported for the ACP-treated relaxor-PT piezoelectric system.[39] It was reported that a small-signal d_{33} and phase angle were enhanced due to the improved domain switching in BF-based ceramics using a combination of ACP and DCP treatment.[40] However, this is in a beginning stage, thus systematic ACP study is required for enhancement of the piezoelectric coefficient and phase angle. As in the ACP study using a single crystal, it is necessary to optimize various parameters such as frequencies, cycles, and temperature to improve the piezoelectric coefficient and phase angle in polycrystalline ceramics.[39–43] In particular, this BTBF-based system requires detailed poling temperature research due to the distortion of the lattice showing a large anisotropic change with temperature below the phase transition temperature.[23] Hence, significantly enhanced piezoelectricity is anticipated in this system by the high-temperature ACP treatment owing to its relaxor ferroelectric nature and interesting crystal symmetry results.

It can be seen that piezoelectric and ferroelectric properties differed significantly with the changing BT/BF ratios, while the electrical properties changed little as a function of the BMT concentration as shown in Figs. 3–5. Almost analogous piezoelectric properties depending on the BMT concentration were observed in all the BTBF series compositions. A similar tendency was also observed in T_{max} as shown in Fig. 6, which varied within 10% as a function of the BMT concentration. Here, it is important to mention that crystal structure remains unchanged for all of the BMT concentrations in all BTBF series as shown in the Appendix. A. It is worthy to mention that the main contributor of large strain and piezoelectricity in the pseudo-cubic symmetry is generally found to be originated from the electric-field-induced phase transition. However, this phenomenon was not observed in the BMT-modified BTBF system and other BF-based solid solution ceramics, as validated by the fact that it maintains a single peak under the applied electric field.[22,44] At this moment, it is unclear why the piezoelectric properties are little tuned by BMT concentration while maintaining the same crystal structure. For this, our current observation is crucial. It was reported that ferroelectricity and piezoelectricity could be attributed to the locally distorted structure in Bi-based ceramics.[23,45,46] The Bi^{3+} ions tend to go off-centered owing to hybridization between their lone pair orbital with the 2p orbitals of oxygen ions. In the BTBF system, the A-site Bi ion off-centering displacement is correlated to the covalent bonding between Bi and O as a function of BT contents.[46] It can be thought that the extent of A- and B-site ions should be changed simultaneously when BMT composition is modified into the BTBF system. This means that local symmetry can be fluctuated by the concentration of B-site (Ti/Mg/Fe) cations and A-site (Ba/Bi) cations. Hence, the elucidation of piezoelectric and ferroelectric properties as a function of BMT concentration could be explained by the local disordering of the cations. For this, Rietveld refinement, electron-density distribution by the maximum entropy method, and pair distribution function analysis are required.[47]

4. Conclusions

In conclusion, the crystal structure and dielectric, ferroelectric, and piezoelectric properties of BMT-modified BTBF systems were systematically investigated by changing the BT/BF ratios and BMT concentration. The noticeable variation of ferroelectric and piezoelectric properties was revealed with changing the BT contents. The analysis of crystal structure, dielectric relaxation, and piezoelectric and ferroelectric properties suggested the dominant ferroelectric order for BF-rich 25BTBF-BMT series, while dominant relaxor-like behavior was revealed for the BT-rich 40BTBF-BMT series. The BT-rich composition series show pseudo-cubic symmetry and strong relaxor-like order, on the other hand, the addition of a higher concentration of BF appears to validate the rhombohedral symmetry and dominant ferroelectric order. Thus, the BF-rich 25BTBF-BMT series leads to the high P_r, E_c, S_{neg}, and low d_{33}*, while the 40BTBF-BMT series show the highest large-signal d_{33}* of 318–384 pm V^{-1}. Based on the analysis of the structural characteristics and overall electrical properties, a feasible aspect of further piezoelectricity enhancement in the 33BTBF-BMT series could be predicted through relaxor ferroelectric order. A significant variation in ferroelectric and piezoelectric properties was not observed with changing the BMT concentration. Interestingly, the tailoring of the piezoelectric and ferroelectric properties without affecting crystal structure by varying BMT concentration was revealed. It might be attributed to the locally distorted symmetry when BMT composition is modified into the BTBF system. This work

suggests that the BTBF-based system with control of the BMT concentration along with BT/BF ratios could serve as a candidate material for various practical applications.

Acknowledgments

The authors would like to thank Nippon Chemical Industrial Co., Ltd., and Sakai Chemical Industry Co., Ltd., for providing the $BiFeO_3$ and $BaTiO_3$ powder. The authors would also like to thank the Graduate Program for Power Energy Professionals, Waseda University, of the Japanese Ministry of Education, Culture, Sports, Science, and Technology (MEXT) WISE Program for its partial support of this work. The synchrotron radiation experiments were conducted with the approval of the Japan Synchrotron Radiation Research Institute (JASRI) (Proposal Nos. 2021A1333, 2021B1311, and 2022A1133).

Appendix A

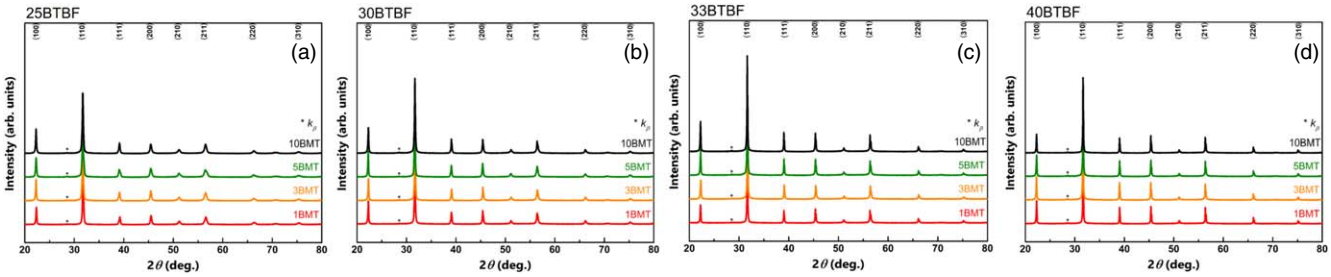

Fig. A·1. (Color online) The XRD patterns of BMT-modified BTBF solid solution: (a) 25BTBF-BMT, (b) 30BTBF-BMT, (c) 33BTBF-BMT, and (d) 40BTBF-BMT series.

Appendix B

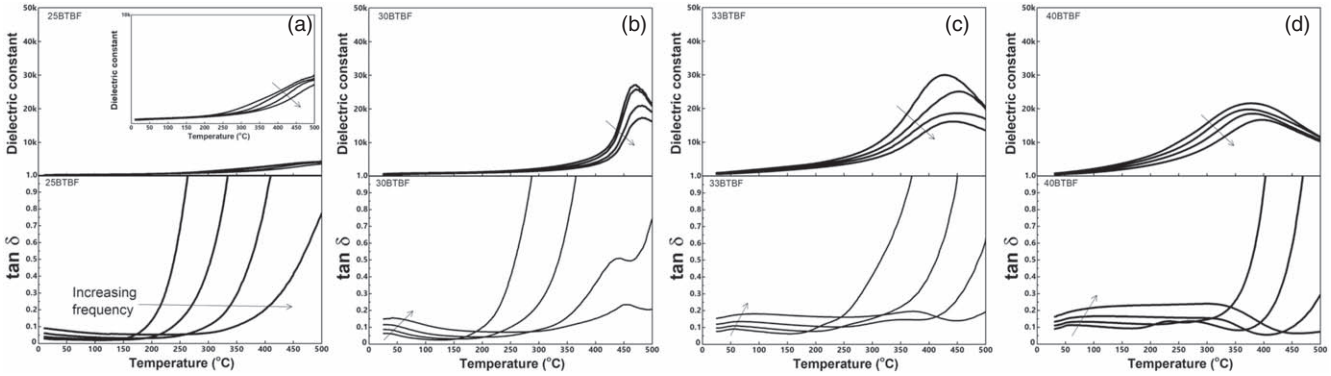

Fig. B·1. The temperature dependence of dielectric constants and losses for 1BMT-modified BTBF solid solution: (a) 25BTBF-1BMT, (b) 30BTBF-1BMT, (c) 33BTBF-1BMT, and (d) 40BTBF-1BMT series, which was measured at frequencies of 1 kHz, 10 kHz, 100 kHz, and 1 MHz.

Appendix C

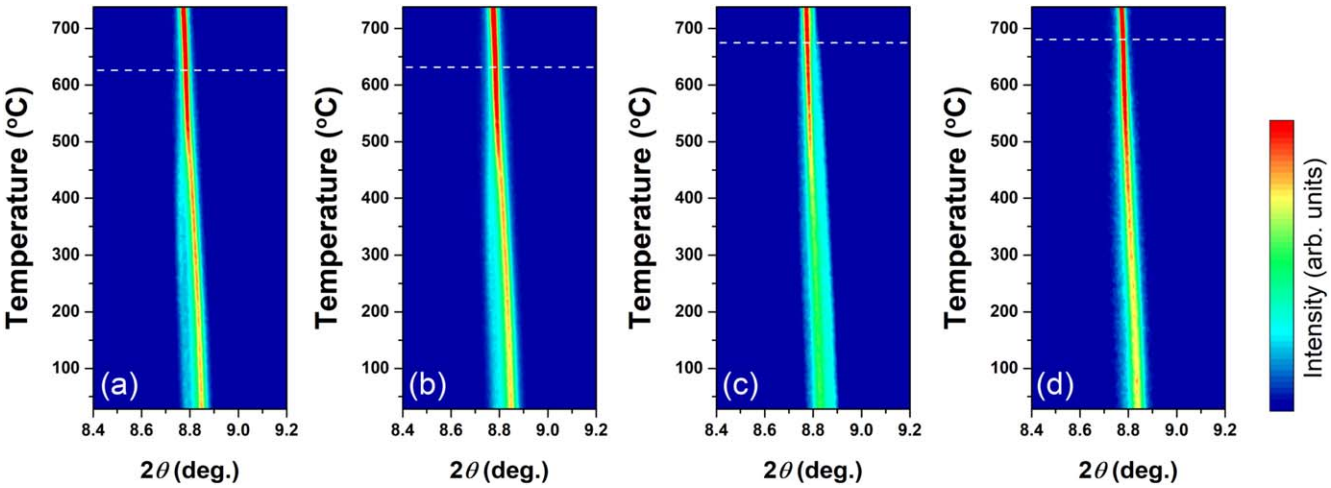

Fig. C·1. (Color online) The profile of 111 peaks under temperature dependence SR-XRD for 25BTBF-BMT solid solution: (a) 25BTBF-1BMT, (b) 25BTBF-3BMT, (c) 25BTBF-5BMT, and (d) 25BTBF-10BMT.

ORCID iDs

Ichiro Fujii https://orcid.org/0000-0003-0207-6415
Sangwook Kim https://orcid.org/0000-0003-2134-1640
Yoshihiro Kuroiwa https://orcid.org/0000-0001-5963-513X

1) B. Jaffe, W. R. Cook Jr., and H. Jaffe, *Piezoelectric Ceramics* (Academic, New York, 1971).
2) G. H. Haertling, J. A. Ceram. Soc. **82**, 797 (1999).
3) K. Uchino, *Piezoelectric Actuator, and Ultrasonic Motors* (Kluwer, Dordrecht, 1997).
4) R. Theissmann, L. A. Schmitt, J. Kling, R. Schierholz, K. A. Schonau, H. Fuess, M. Knapp, H. Kungl, and M. J. Hoffmann, J. Appl. Phys. **102**, 024111 (2007).
5) T. Asada and Y. Koyama, Phys. Rev. B **75**, 214111 (2007).
6) S. Wada, S.-E. Park, L. E. Cross, and T. R. Shrout, Ferroelectrics **221**, 147 (1999).
7) D. Lin, S. Zhang, Z. Li, F. Li, Z. Xu, S. Wada, J. Luo, and T. R. Shrout, J. Appl. Phys. **110**, 084110 (2011).
8) S. Wada, K. Yamato, P. Pulpan, N. Kumada, B.-Y. Lee, T. Iijima, C. Moriyoshi, and Y. Kuroiwa, J. Appl. Phys. **108**, 094114 (2010).
9) I. Fujii, K. Yamato, M. Shimada, J. Hayashi, H. Yabuta, M. Kubota, T. Fukui, K. Nakashima, N. Kumada, and S. Wada, Key Eng. Mater. **485**, 31 (2011).
10) I. Fujii et al., Jpn. J. Appl. Phys. **50**, 09ND07 (2011).
11) R. Mitsui, I. Fujii, K. Nakashima, N. Kumada, Y. Kuroiwa, and S. Wada, Ceram. Int. **39**, S695 (2013).
12) H. Yabuta, M. Shimada, T. Watanabe, J. Hayashi, M. Kubota, K. Miura, T. Fukui, I. Fujii, and S. Wada, Jpn. J. Appl. Phys. **51**, 09LD04 (2012).
13) R. Mitsui, I. Fujii, K. Nakashima, N. Kumada, Y. Kuroiwa, and S. Wada, J. Ceram. Soc. Jpn. **121**, 855 (2013).
14) R. Mitsui et al., Key Eng. Mater. **566**, 59 (2013).
15) H. Nam, S. Kim, T. Aizawa, I. Fujii, S. Ueno, and S. Wada, Ceram. Int. **44**, S199 (2018).
16) T. Rojac, M. Kosec, B. Budic, N. Setter, and D. Damjanovic, J. Appl. Phys. **108**, 074107 (2010).
17) S. Kim, G. P. Khanal, S. Ueno, C. Moriyoshi, Y. Kuroiwa, and S. Wada, J. Appl. Phys. **122**, 014103 (2017).
18) S. Kim, G. P. Khanal, H.-W. Nam, J. Fujii, S. Ueno, C. Moriyoshi, Y. Kuroiwa, and S. Wada, J. Appl. Phys. **122**, 164105 (2017).
19) S. O. Leontsev and R. E. Eitel, J. Am. Ceram. Soc. **92**, 2957 (2009).
20) A. Singh, A. Kumar, and D. Pandey, J. Appl. Phys. **124**, 224101 (2018).
21) I. Calisir and D. A. Hall, J. Mater. Chem. C **6**, 134 (2018).
22) I. Fujii, R. Iizuka, Y. Nakahira, Y. Sunada, S. Ueno, K. Nakashima, E. Magome, C. Moriyoshi, Y. Kuroiwa, and S. Wada, Appl. Phys. Lett. **108**, 172903 (2016).
23) Y. Kuroiwa, S. Kim, I. Fujii, S. Ueno, Y. Kakahira, C. Moriyoshi, Y. Sato, and S. Wada, Commun. Mater. **1**, 71 (2020).
24) Y. Gao, K. Uchino, and D. Viehland, J. Appl. Phys. **101**, 114110 (2007).
25) H. Nam, I. Fujii, S. Kim, T. Aizawa, S. Ueno, and S. Wada, J. Ceram. Soc. Jpn. **127**, 369 (2019).
26) A. Bencan, G. Drazic, H. Ursic, B. Jancar, M. Makarovic, M. Komelj, and T. Rojac, Nat. Commun. **11**, 1762 (2020).
27) J. Koruza, A. J. Bell, T. Frömling, K. G. Webber, K. Wang, and J. Rödel, J. Materiomics. **4**, 13 (2018).
28) S. Zhang, B. Malic, J.-F. Li, and J. Rödel, J. Mater. Res. **36**, 985 (2021).
29) K. Shibata, R. Wang, T. Tou, and J. Koruza, MRS Bull. **43**, 612 (2018).
30) V.-Q. Naguyen, H.-S. Han, K.-J. Kim, D.-D. Dang, K.-K. Ahn, and J.-S. Lee, J. Alloys Compd. **511**, 237 (2012).
31) S.-T. Zhang, A. B. Kounga, E. Aulbach, T. Granzow, W. Jo, H.-J. Kleebe, and J. Rödel, J. Appl. Phys. **103**, 034107 (2008).
32) C. Li, T. Zheng, and J. Wu, Acta Mater. **206**, 116601 (2021).
33) S. Zhang, J. B. Lim, H. J. Lee, and T. R. Shrout, IEEE Trans. Ultrason. Ferroelectr. Freq. Control **56**, 1523 (2009).
34) Y. Hosono and Y. Yamashita, IEEE Trans. Ultrason. Ferroelectr. Freq. Control **52**, 1823 (2005).
35) S. Murakami, N. T. A. F. Ahmed, D. Wang, A. Feteira, D. C. Sinclair, and I. M. Reaney, J. Eur. Ceram. Soc. **38**, 4220 (2018).
36) S. Murakami, D. Wang, A. Mostaed, A. Khesro, A. Feteira, D. C. Sinclair, Z. Fan, X. Tan, and I. M. Reaney, J. Am. Ceram. Soc. **101**, 5428 (2018).
37) K. Uchino and S. Nomura, Ferroelectrics **44**, 55 (1982).
38) S. Kim, H. Nam, and I. Calisir, Materials. **15**, 4388 (2022).
39) Y. Sun, T. Karaki, and Y. Yamashita, Jpn. J. Appl. Phys. **61**, SB0802 (2022).
40) S. Kim, G. P. Khanal, H. Nam, I. Fujii, S. Ueno, and S. Wada, J. Ceram. Soc. Jpn. **127**, 353 (2019).
41) C. Luo, H. Wan, W.-Y. Chang, Y. Yamashita, A. R. Paterson, J. Jones, and X. Jiang, Appl. Phys. Lett. **115**, 192904 (2019).
42) Y. Sun, T. Karaki, T. Fujii, and Y. Yamashita, Jpn. J. Appl. Phys. **59**, SPPD08 (2020).
43) C. Luo, T. Karaki, Y. Sun, Y. Yamashita, and J. Xu, Jpn. J. Appl. Phys. **59**, SPPD07 (2020).
44) S. Kim, G. P. Khanal, H. Nam, M. Kim, I. Fujii, S. Ueno, C. Moriyoshi, Y. Kuroiwa, and S. Wada, J. Ceram. Soc. Jpn. **126**, 316 (2018).
45) S. Kim, H. Nam, I. Fujii, S. Ueno, C. Moriyoshi, Y. Kuroiwa, and S. Wada, Scr. Mater. **205**, 114176 (2021).
46) S. Kim, H. Nam, I. Fujii, S. Ueno, C. Moriyoshi, Y. Kuroiwa, and S. Wada, Jpn. J. Appl. Phys. **60**, SFFD01 (2021).
47) Y. Yoneda and Y. Noguchi, Jpn. J. Appl. Phys. **60**, SFFA08 (2021).